Journal of Nuclear Medicine, published on March 10, 2016 as doi:10.2967/jnumed.115.166918

Comparison of Tumor Uptake Heterogeneity Characterization between Static and Parametric ^{18}F-FDG PET Images in Non-Small Cell Lung Cancer

Florent Tixier[1], Dennis Vriens[2], Catherine Cheze-Le Rest[1], Mathieu Hatt[3], Jonathan A Disselhorst[4], Wim JG Oyen[5], Lioe-Fee de Geus-Oei[2], Eric P Visser[6], Dimitris Visvikis[3]

[1]Poitiers University Hospital, Department of Nuclear Medicine, EE DACTIM, Poitiers, France

[2]Leiden University Medical Centre (LUMC), Department of Radiology, Leiden, the Netherlands

[3]INSERM, UMR 1101, LaTIM, CHRU Morvan, Brest, France

[4]Werner Siemens Imaging Center, Department of Preclinical Imaging, University of Tübingen, Tübingen, Germany

[5]Institute of Cancer Research, Royal Marsden NHS Trust, London, United Kingdom

[6]Department of Radiology, Radboud University Medical Center, Nijmegen, Netherlands

Corresponding author:
TIXIER Florent
DACTIM,
CHU Miletrie, 86000 Poitiers, France
Tel: +33 (0)549-444-774
Email: florent.tixier@chu-poitiers.fr

Short running title: SUV vs MRGlu based tumor heterogeneity

Word count: 4987

Keywords: Intra-tumor heterogeneity, parametric PET images, non-small cell lung cancer

ABSTRACT

^{18}F-2-fluoro-2-deoxy-D-glucose (^{18}F-FDG) positron emission tomography (PET) is well established in the field of oncology for diagnosis and staging purposes, while increasingly is being used for therapy response assessment and prognosis. Many quantitative indices can be used to characterize tumors in ^{18}F-FDG PET images, such as the maximum of standardized radiotracer uptake (SUV_{max}), metabolically active tumor volume (MATV), total lesion glycolysis (TLG) or more recently proposed intra-tumor uptake heterogeneity features. Although most PET data considered within this context concerns the analysis of activity distribution images obtained from one static acquisition, parametric images generated from dynamic acquisitions and reflecting radiotracer kinetics may provide additional information. The purpose of this study was to quantify differences between volumetric, uptake and heterogeneity features extracted from static and parametric PET images in non-small cell lung carcinoma (NSCLC) in order to provide insight on the potential added value of parametric images. **Methods:** Dynamic ^{18}F-FDG PET/CT acquisitions were performed in twenty therapy-naive NSCLC patients planned for primary surgical resection. Both static and parametric PET images were analyzed with quantitative parameters (MATV, SUV_{max}, SUV_{mean}, heterogeneity) extracted from the segmented tumors. Differences were investigated using Spearman's rank correlation coefficients (rs) and Bland-Altman analysis. **Results**: MATV was slightly smaller in static images (-2±7%), but the difference was not significant (p=0.14). All derived parameters, including those characterizing tumor functional heterogeneity, were highly correlated between static and parametric images (rs=0.70-0.98, p≤0.0006) exhibiting differences of <±25%. **Conclusion**: In NSCLC primary tumors, parametric and static baseline ^{18}F-FDG PET images provided highly

correlated quantitative features for both standard (MATV, SUV_{max}, SUV_{mean}) and heterogeneity quantification. Consequently, heterogeneity quantification on parametric images does not seem to provide significant complementary information compared to static SUV images.

INTRODUCTION

^{18}F-2-fluoro-2-deoxy-D-glucose (^{18}F-FDG) positron emission tomography (PET) is increasingly used for tumor detection, initial staging, treatment monitoring and planning, therapeutic response evaluation, and prognosis *(1-4)*. Within this context quantitative features can be used from either baseline PET images or by comparison between pre- and per/post-treatment scans. The maximum of standardized uptake value (SUV_{max}) from static images (55-65 mins after injection) is the most commonly used, although it does not provide a comprehensive tumor characterization and may therefore be limited for all clinical applications *(5,6)*. Additional standard features include mean SUV (SUV_{mean}), the metabolically active tumor volume (MATV) and total lesion glycolysis (TLG, defined as MATV x SUV_{mean}) *(7)*. Most ^{18}F-FDG PET derived features are sensitive to physiological parameters such as body composition and blood glucose concentration that may add confounding factors in inter and/or intra patient comparisons *(8)*. Recently, PET intra-tumor heterogeneity characterization has demonstrated a potential added predictive and prognostic value over simple SUV measurements *(9,10)*. However, these studies have to date been exclusively based on static PET acquisitions. Whereas static whole body ^{18}F-FDG PET acquisitions are the most commonly used in clinical practice, an alternative consists in analyzing radiotracer kinetics to provide fully quantitative information *(10)*, such as the metabolic rate of glucose (MRGlu). Amongst kinetic models, Patlak analysis is considered as a gold standard for modelling tissue time-activity concentration (TAC) curves derived from dynamic ^{18}F-FDG PET images *(11,12)*.

The fully quantitative parameters derived using such approaches have been previously shown to be useful in patient management *(13)*, with observed differences

between static SUV and parametric MRGlu images *(14,15)*. Firstly, SUV images reflect only the total activity, without any distinction between metabolized and unmetabolized ^{18}F-FDG uptake. In the Patlak analysis, the time integral of the input TAC divided by the plasma concentration is plotted on the horizontal axis versus the activity on the vertical axis, while SUV approximates this integral by normalizing static activity concentrations using patient weight and injected dose.

Cheebsumon, et al. observed different MATVs when delineated in static or dynamic ^{18}F-FDG images *(16)*, whereas Visser, et al. observed that MRGlu maps led to significantly smaller MATVs than SUV-based images *(17)*. The magnitude of these differences can be explained by the delineation methodology used. Threshold-based methods have been previously shown to lack robustness relative to varying image properties (noise, contrast) *(18)*, which is the case for static *vs.* parametric PET images *(17)*.

The potential interest of dynamic imaging for the characterization of intra-tumor heterogeneity based on texture analysis has not been previously evaluated. A recent review referred to the potential of features derived from parametric maps calculated using kinetic analysis in conjunction with the temporal evolution of intra-tumor tracer uptake distribution *(19)*, without an explicit evaluation in a given patient cohort. The present study aims to assess the potential complementary value of dynamic acquisitions and derived quantitative parametric images for intra-tumor heterogeneity characterization using ^{18}F-FDG PET. Our main objective was to quantify the potential differences between newly proposed intra-tumor heterogeneity characterization features from static SUV and parametric MRGlu ^{18}F-FDG PET images derived using the Patlak linearisation approach *(11)*. For comparison purposes, the

analysis was extended to other standard PET image derived indices such as SUV_{max}, SUV_{mean}, TLG and MATV.

MATERIALS AND METHODS

Patients

Twenty therapy-naive patients with limited-stage non-small cell lung carcinoma (NSCLC) and planned for primary surgical resection, were prospectively recruited. Tumors with at least 30 mm maximum diameter were considered in order to reduce the potential impact of partial volume effects (PVE) and respiratory motion on the quantitative measurements considered *(20)*. The study was approved by the Medical Ethics Review Committee of The Radboud University Nijmegen Medical Centre and all patients gave a written informed consent. Patient characteristics are summarized in Table 1.

^{18}F-FDG PET Acquisitions and Image Reconstruction

All 20 patients underwent a dynamic PET acquisition in list-mode for 60 min using a Biograph Duo scanner (Siemens Healthcare) in a single bed position (159 mm axial length) after intravenous injection of an average 3.3 MBq/kg using an infusion pump (8 mL ^{18}F-FDG at 0.2 mL/s followed by 40 mL saline flush at 8.0 mL/s). A low-dose CT acquisition (40 mA and 130 kV) over the same area covered by the PET scan, was used for PET attenuation correction and anatomical reference. The CT transaxial matrix size was 512x512 (0.98x0.98 mm^2), while the CT slice width was 3 mm.

PET data were reconstructed using a 45-frame protocol (10s delay after ^{18}F-FDG injection, 16×5s, 4x10s, 4×20s, 4×30s, 4x60s, 4x120s, 1x150s and 8×300s). Each of the

45 frames was reconstructed using ordered subsets expectation maximization in two dimensions (OSEM 2D) with 4 iterations and 16 subsets in a 256×256×53 image matrix (voxel size 2.65×2.65×3.00mm^3) followed by post-filtering with an isotropic 5mm full-width-at-half-maximum (FWHM) 3D Gaussian filter. CT based attenuation correction using a bilinear transformation of Hounsfield units to the PET energy attenuation values, a delayed window based randoms correction, single scatter simulation based scatter correction and decay correction were applied. No partial volume or respiratory motion corrections were considered.

The last time frame of the dynamic series (55-60min post-injection (p.i.)) was used to generate the SUV images. All voxel values [Bq/mL] were normalized to the administered activity [Bq] per body weight [g]. Residual activity in the infusion system was accounted for (*i.e.* SUV [g/mL]).

MRGlu values were calculated on a voxel-by-voxel basis, deriving MRGlu parametric maps, based on the standard 2-compartment ^{18}F-FDG model with trapping in the linear approximation (Patlak analysis) *(12)* according to:

$$MRGlu = \frac{K_1 k_3}{k_2 + k_3} \frac{C_{p,glu}}{LC_{FDG}} = K_i \frac{C_{p,glu}}{LC_{FDG}}$$

where, K_1, k_2, and k_3 are the three rate constants of the two compartment model, K_i [ml/g/min] is the ^{18}F-FDG influx constant, $C_{p,glu}$ is the plasma glucose concentration, and LC_{FDG} is the lumped constant (=1). For the tissue TAC curves, the images from frames 38-45 (*i.e.* 20-60 min p.i.) were used, since for all tumors investigated the Patlak curves approached a straight line at 15-20 min p.i.. An image derived input function (plasma TAC) was determined by considering the mean activity concentration in a manually

drawn 3D volume of interest in the thoracic ascending aorta (whole blood). No plasma to whole blood ratio or PVE corrections were applied. Voxelwise K_i values were subsequently determined by linear regression analysis on the Inveon Research Workplace version 3 (Siemens Healthcare, Knoxville, USA), using the tissue TAC and the image-derived whole-blood TAC. Using the derived parametric images the Metabolic Rate Volume (MRV = $MRGlu_{mean}$ × volume), used to denote the parametric equivalent of TLG in SUV images, was also derived for each tumor volume.

Image Analysis

For all patients, the primary tumor MATV was delineated on the static SUV and parametric PET images. The automatic Fuzzy Locally Adaptive Bayesian (FLAB) algorithm previously validated for accuracy, robustness and reproducibility in PET *(21,22)*, was used to minimize the delineation approach impact on the extracted features. From these delineated volumes, the following features were extracted from both static and parametric images: MATV, maximum value (SUV_{max} and Ki_{max}), metabolic volume products (TLG and MRV), and heterogeneity parameters, including the area under the curve of the cumulative intensity histogram (CIH_{AUC}) *(23)* and textural features at both local and regional scales using previously optimized parameters (quantization into 64 grey-levels) *(24)*. CIH_{AUC} is calculated by considering all tumor voxels, consequently providing a global quantification of the tumor heterogeneity. Local heterogeneity features were computed using a single co-occurrence matrix over all 13 spatial directions in 3D *(20)*. They highlight intensity variations between contiguous voxels at the local scale and include homogeneity (H),

entropy (E) and dissimilarity (D). Regional heterogeneity measurements were computed using matrices that link groups of intra-tumor voxels with similar intensity. They include high intensity emphasis (HIE) and zone percentage (ZP) *(24)*. Most heterogeneity textural features used in this study were chosen according to previously published results regarding their reproducibility *(25)* and robustness to both functional tumor volume delineation approaches and PVE *(18,26)*.

Statistical Analysis

Statistical analysis was performed using the MedCalc^{TM} software, (MedCalc Software, Belgium). The statistics of each parameter's distribution in both images were reported using the 1st and 3rd quartile, as well as the median. The Kolmogorov-Smirnov test was used to assess the normality of distributions. The agreement between parameters from static and parametric images was assessed using the Spearman's rank coefficient (ρ) and differences were quantified using a Bland-Altman analysis, reporting the mean±SD and 95% confidence intervals (CI) of the differences and the upper (UL) and lower limits (LL) defined as 1.96 × standard deviation (SD) after a log transformation applied to parameters with a non- normal distribution. Note that for SUV_{max} (or Ki_{max}) and TLG (or MRV), only correlation coefficients are reported, since the measures are not directly comparable between the two image types given the differences in units. P-values <0.05 were considered significant throughout the analyses.

RESULTS

Figure 1 shows delineated tumor examples in both images including differences in the corresponding image indices considered. All features were normally distributed with the exception of MATV and TLG/MRV (Table 2). MATVs measured on static and parametric images were highly correlated (rs=0.96, p<0.0001, 95%CI 0.90-0.99) (Table 3). Slightly smaller MATVs were obtained on static compared to the corresponding parametric images, with non-statistically significant differences (-2±7%, p=0.14, upper limits (UL) and lower limits (LL) of +11% and -15% respectively) (Table 3, Figure 2A). The smallest and largest absolute volume differences were 0 cm^3 and 26.5 cm^3 respectively, which was obtained for a very large tumor (>145 cm^3 *vs* 115 cm^3 in the parametric *vs* static images).

As Figure 2B shows SUV_{max} and Ki_{max} were highly correlated (rs=0.9, p<0.0001, 95% CI 0.76-0.99). Similarly, TLG and MRV were highly correlated with a Spearman's rank correlation coefficient of 0.98 (95% CI 0.94-0.99, p<0.0001, Figure 2C). Intra-tumor heterogeneity parameters on the static and parametric images were also correlated (rs between 0.7 and 0.91, p≤0.0006), with <21% SD and UL/LL within the ±40% range, which are similar to the physiological reproducibility limits previously measured on test-retest baseline PET images for such parameters *(22, 25)*. The heterogeneity parameters showing the lowest variability with respect to static *vs.* parametric PET images were entropy (0.3±2.1%, UL/LL of +3.8/-4.4%, Figure 2D) and zone percentage (+1.0±3.7%, UL/LL of +8.2%/-6.1%, Figure 2E). Homogeneity led to slightly larger differences (+0.6±11.9%, UL/LL of +24.0%/-22.7%), whereas dissimilarity had a similar behavior as CIH_{AUC} with 16-17% SD, and UL/LL around ±30-35% (Figure 2F). Finally, the parameter that exhibited the largest difference was HIE with +0.3±20.9% (UL/LL of +41.3%/-40.6%, Table 3).

DISCUSSION

There is currently an increasing interest in PET intra-tumor heterogeneity characterization and its potential added value for diagnosis, therapy response and survival analysis. It has already been already shown that in NSCLC, intra-tumor heterogeneity in whole body static ^{18}F-FDG PET has a complementary prognostic value relative to the metabolic functional volume *(20,27)*, but also a predictive value in the case of exclusive chemotherapy treatment *(28)*. On the other hand, there are a number of unanswered questions concerning the robustness of these heterogeneity parameters and their underlying biological significance. Some of these features, including those used in this study, have been shown to be robust to physiological reproducibility *(25,29)*. In terms of their biological significance, we have previously shown that tumor blood flow highly correlated with different scale tumor heterogeneity indices extracted from ^{18}F-FDG PET images in colorectal cancer *(30)*. In order to further evaluate the robustness of intra-tumor heterogeneity characterization in ^{18}F-FDG PET for NSCLC, the goal of this study was for the first time ever to compare intra-tumor heterogeneity parameters between standard static acquisitions and quantitative parametric ^{18}F-FDG PET images. The underlying goal of this original comparison was to provide some insight into the potential added information that parametric images may give relative to standard clinical PET acquisitions.

Firstly, the use of a robust delineation approach allowed to overcome potential robustness issues previously observed *(21)* in the determination of MATVs measured in static *vs.* parametric PET images (-2±7% and limits between 11-15%). The observed variations are well within the range of upper and lower physiological reproducibility

limits previously determined for FLAB at ±30% *(22)*, and substantially lower than those previously reported using less robust delineation methods based on fixed thresholding *(17)*. Fixed thresholding has been shown to lack robustness and be very sensitive to tumor contrast *(31)*. The higher contrast in parametric images *(32)* may consequently explain such MATV differences that were not observed in the present study using a more robust delineation algorithm.

We also found that maximum intensity (SUV_{max} and Ki_{max}) as well as total activity (TLG and MRV) measurements were highly correlated between static and parametric images ($rs \geq 0.9$). This is in line with previously reported results for renal cell carcinoma metastases by Freedman, et al. *(14)* and for breast cancer by Doot, et al. *(33)*. Both found a high correlation ($r > 0.95$) between SUV_{max} and Ki_{max} on baseline ^{18}F-FDG PET scans.

Most of the uptake heterogeneity features considered in the present study showed high correlation ($rs \geq 0.7$, $p \leq 0.0006$) when obtained using static or parametric PET images, with differences <±25% range, except for HIE (±40%) and dissimilarity (±30%). In particular, entropy and zone percentage values were very similar (<±5% and <±9% respectively), providing further evidence for the robustness of these parameters in intra-tumor heterogeneity characterization *(18, 26)*. The highest differences associated with HIE may be explained by its previously demonstrated lower robustness to PVE (mean difference of -20.6±18.8 between PVE and non-PVE corrected images) *(18)*.

Our results suggest that the observed differences in quantitative measurements of intra-tumor heterogeneity between static and parametric ^{18}F-FDG images can be mostly attributed to variabilities in image characteristics and noise

rather than substantial differences in the actual intra-tumor uptake spatial distribution (Figure 1). This in turn supports the hypothesis that with respect to intra-tumor heterogeneity characterization the parametric images provide similar information to static SUV images on a ^{18}F-FDG PET baseline scan.

Based on the Patlak analysis assumptions and the use of the baseline scan only, the hypotheses in this work are that the unmetabolized component of ^{18}F-FDG is negligible at later times and the ratio of the injected dose / patient weight is proportional to the area under the curve of the arterial input function. If one considers the comparison between a baseline scan and an early or late scan, for instance within the context of early/late therapy response monitoring, the conclusions may be different. Although beyond the objectives of this work, in such a comparative framework parametric images may eventually provide useful additional information. For example, it has been previously demonstrated within the context of early therapy response prediction in locally advanced breast cancer that dynamic PET scans provided clinical added value over static SUV measurements, leading to significantly higher predictive accuracy *(34)*. This study was however based on the comparison of SUV measurements only and did not include more advanced tumor characterization metrics (volume, heterogeneity).

Our study is limited by the small number of patients and the consideration of NSCLC patients with large lesions (> 3cm). Despite the limited number of patients, the small mean parameter differences observed suggest that similar information on tumor heterogeneity can be derived from the static and parametric baseline ^{18}F-FDG PET images. Given these small differences a more substantial patient cohort is needed to

confirm the statistical significance of these results. Concerning the limit on the lesions' size it was chosen to reduce the influence of both respiratory motion and PVE. Previous studies have shown variabilities on heterogeneity features as a result of respiratory gating *(35,36)*, although no statistically significant differences were seen on the PET heterogeneity parameters considered in this study *(37)*. In addition, the majority of the lesions in this study (85%) were located in the upper lung lobes which are less influenced by respiratory motion.

The choice of NSCLC can be also a limitation since the lung tissue is mostly metabolically non active, thus the background is low, and the fraction of unmetabolized ^{18}F-FDG is also very low. Our present conclusions for NSCLC cannot therefore be extended to pathologies in tissues with higher background levels (e.g. liver metastases) or near "reservoirs" of metabolic inactive ^{18}F-FDG, for example in urine or even blood (especially in end stage renal failure patients).

Although the high correlation between features extracted from static and parametric PET images suggest that there is no significant complementary information to be derived from parametric ^{18}F-FDG PET images, further validation studies are required in order to compare the actual predictive or prognostic value of static *vs.* parametric images for patient response or overall survival in NSCLC.

CONCLUSIONS

In NSCLC, parametric and static SUV ^{18}F-FDG PET images provided similar and highly correlated tumor derived characterization parameters considering a single baseline scan. More specifically similar correlation and small differences were found

for metrics such as entropy and zone percentage quantifying intra-tumor uptake spatial distribution heterogeneity. Despite the limited number of patients and the lack of consideration for respiratory motion, the present study suggests that there does not seem to be any added value from dynamic ^{18}F-FDG PET acquisitions considering the role of intra-tumor heterogeneity analysis on a single baseline ^{18}F-FDG PET image within the context of patient management in NSCLC.

ACKNOWLEDGEMENTS

This study was supported by a grant from the Ligue Contre le Cancer (Finistere and Côtes d'Armor Committees). No other potential conflicts of interest relevant to this article are to be reported.

REFERENCES

1. Czernin J, Benz MR, Allen-Auerbach MS. PET/CT imaging: The incremental value of assessing the glucose metabolic phenotype and the structure of cancers in a single examination. *Eur J Radiol.* 2010;73:470-480.

2. Gregoire V, Haustermans K, Geets X, Roels S, Lonneux M. PET-based treatment planning in radiotherapy: a new standard? *J Nucl Med.* 2007;48(suppl 1):68S-77S.

3. Harry VN, Semple SI, Parkin DE, Gilbert FJ. Use of new imaging techniques to predict tumour response to therapy. *Lancet Oncol.* 2010;11:92-102.

4. Jadvar H, Alavi A, Gambhir SS. 18F-FDG uptake in lung, breast, and colon cancers: molecular biology correlates and disease characterization. *J Nucl Med.* 2009;50:1820-1827.

5. Hatt M, Visvikis D, Pradier O, Cheze-le Rest C. Baseline (1)(8)F-FDG PET image-derived parameters for therapy response prediction in oesophageal cancer. *Eur J Nucl Med Mol imaging.* 2011;38:1595-1606.

6. Wieder HA, Ott K, Lordick F, et al. Prediction of tumor response by FDG-PET: comparison of the accuracy of single and sequential studies in patients with adenocarcinomas of the esophagogastric junction. *Eur J Nucl Med Mol imaging.* 2007;34:1925-1932.

7. Larson SM, Erdi Y, Akhurst T, et al. Tumor Treatment Response Based on Visual and Quantitative Changes in Global Tumor Glycolysis Using PET-FDG Imaging. The Visual Response Score and the Change in Total Lesion Glycolysis. *Clin positron imaging.* 1999;2:159-171.

8. Boellaard R. Standards for PET image acquisition and quantitative data analysis. *J Nucl Med.* 2009;50(suppl 1):11S-20S.

9. Rizk NP, Tang L, Adusumilli PS, et al. Predictive value of initial PET-SUVmax in patients with locally advanced esophageal and gastroesophageal junction adenocarcinoma. *J Thorac Oncol.* 2009;4:875-879.

10. Hoekstra CJ, Paglianiti I, Hoekstra OS, et al. Monitoring response to therapy in cancer using [18F]-2-fluoro-2-deoxy-D-glucose and positron emission tomography: an overview of different analytical methods. *Eur J Nucl Med.* 2000;27:731-743.

11. Vriens D, Visser EP, de Geus-Oei LF, Oyen WJ. Methodological considerations in quantification of oncological FDG PET studies. *Eur J Nucl Med Mol imaging.* 2010;37:1408-1425.

12. Patlak CS, Blasberg RG, Fenstermacher JD. Graphical evaluation of blood-to-brain transfer constants from multiple-time uptake data. *J Cereb blood flow Metab.* 1983;3:1-7.

13. Cheebsumon P, Velasquez LM, Hoekstra CJ, et al. Measuring response to therapy using FDG PET: semi-quantitative and full kinetic analysis. *Eur J Nucl Med Mol imaging.* 2011;38:832-842.

14. Freedman NM, Sundaram SK, Kurdziel K, et al. Comparison of SUV and Patlak slope for monitoring of cancer therapy using serial PET scans. *Eur J Nucl Med Mol imaging.* 2003;30:46-53.

15. Weber WA. Use of PET for monitoring cancer therapy and for predicting outcome. *J Nucl Med.* 2005;46:983-995.

16. Cheebsumon P, van Velden FH, Yaqub M, et al. Measurement of metabolic tumor volume: static versus dynamic FDG scans. *EJNMMI Res.* 2011;1:35.

17. Visser EP, Philippens ME, Kienhorst L, et al. Comparison of tumor volumes derived from glucose metabolic rate maps and SUV maps in dynamic 18F-FDG PET. *J Nucl Med.* 2008;49:892-898.

18. Hatt M, Tixier F, Cheze Le Rest C, Pradier O, Visvikis D. Robustness of intratumour (1)(8)F-FDG PET uptake heterogeneity quantification for therapy response prediction in oesophageal carcinoma. *Eur J Nucl Med Mol imaging.* 2013;40:1662-1671.

19. El Naqa I. The role of quantitative PET in predicting cancer treatment outcomes. *Clinical and translational imaging.* 2014;2:305-320.

20. Hatt M, Majdoub M, Vallieres M, et al. 18F-FDG PET uptake characterization through texture analysis: investigating the complementary nature of heterogeneity and functional tumor volume in a multi-cancer site patient cohort. *J Nucl Med.* 2015;56:38-44.

21. Hatt M, Cheze Le Rest C, Albarghach N, Pradier O, Visvikis D. PET functional volume delineation: a robustness and repeatability study. *Eur J Nucl Med Mol imaging.* 2011;38:663-672.

22. Hatt M, Cheze-Le Rest C, Aboagye EO, et al. Reproducibility of 18F-FDG and 3'-deoxy-3'-18F-fluorothymidine PET tumor volume measurements. *J Nucl Med.* 2010;51:1368-1376.

23. van Velden FH, Cheebsumon P, Yaqub M, et al. Evaluation of a cumulative SUV-volume histogram method for parameterizing heterogeneous intratumoural FDG uptake in non-small cell lung cancer PET studies. *Eur J Nucl Med Mol imaging.* 2011;38:1636-1647.

24. Tixier F, Le Rest CC, Hatt M, et al. Intratumor heterogeneity characterized by textural features on baseline 18F-FDG PET images predicts response to concomitant radiochemotherapy in esophageal cancer. *J Nucl Med.* 2011;52:369-378.

25. Tixier F, Hatt M, Le Rest CC, Le Pogam A, Corcos L, Visvikis D. Reproducibility of tumor uptake heterogeneity characterization through textural feature analysis in 18F-FDG PET. *J Nucl Med.* 2012;53:693-700.

26. Galavis PE, Hollensen C, Jallow N, Paliwal B, Jeraj R. Variability of textural features in FDG PET images due to different acquisition modes and reconstruction parameters. *Acta Oncol.* 2010;49:1012-1016.

27. Tixier F, Hatt M, Valla C, et al. Visual versus quantitative assessment of intratumor 18F-FDG PET uptake heterogeneity: prognostic value in non-small cell lung cancer. *J Nucl Med.* 2014;55:1235-1241.

28. Cook GJ, O'Brien ME, Siddique M, et al. Non-Small Cell Lung Cancer Treated with Erlotinib: Heterogeneity of F-FDG Uptake at PET-Association with Treatment Response and Prognosis. *Radiology.* 2015;276:883–893.

29. Willaime JM, Turkheimer FE, Kenny LM, Aboagye EO. Quantification of intra-tumour cell proliferation heterogeneity using imaging descriptors of 18F fluorothymidine-positron emission tomography. *Phys Med Biol.* 2013;58:187-203.

30. Tixier F, Groves AM, Goh V, et al. Correlation of intra-tumor 18F-FDG uptake heterogeneity indices with perfusion CT derived parameters in colorectal cancer. *PLoS One.* 2014;9:e99567.

31. Hatt M, Cheze le Rest C, Turzo A, Roux C, Visvikis D. A fuzzy locally adaptive Bayesian segmentation approach for volume determination in PET. *IEEE Trans Med Imaging.* 2009;28:881-893.

32. Sayre GA, Franc BL, Seo Y. Patient-Specific Method of Generating Parametric Maps of Patlak K(i) without Blood Sampling or Metabolite Correction: A Feasibility Study. *Int J Mol imaging.* 2011;2011:1-12.

33. Doot RK, Dunnwald LK, Schubert EK, et al. Dynamic and static approaches to quantifying 18F-FDG uptake for measuring cancer response to therapy, including the effect of granulocyte CSF. *J Nucl Med.* 2007;48:920-925.

34. Dunnwald LK, Doot RK, Specht JM, et al. PET tumor metabolism in locally advanced breast cancer patients undergoing neoadjuvant chemotherapy: value of static versus kinetic measures of fluorodeoxyglucose uptake. *Clin Cancer Res.* 2011;17:2400-2409.

35. Vaidya M, Creach KM, Frye J, Dehdashti F, Bradley JD, El Naqa I. Combined PET/CT image characteristics for radiotherapy tumor response in lung cancer. *Radiother Oncol.* 2012;102:239-245.

36. Yip S, McCall K, Aristophanous M, Chen AB, Aerts HJ, Berbeco R. Comparison of texture features derived from static and respiratory-gated PET images in non-small cell lung cancer. *PLoS One.* 2014;9:e115510.

37. Grootjans W, Hermsen R, der Heijden EH, et al. The impact of respiratory gated positron emission tomography on clinical staging and management of patients with lung cancer. *Lung cancer.* 2015;90:217-223.

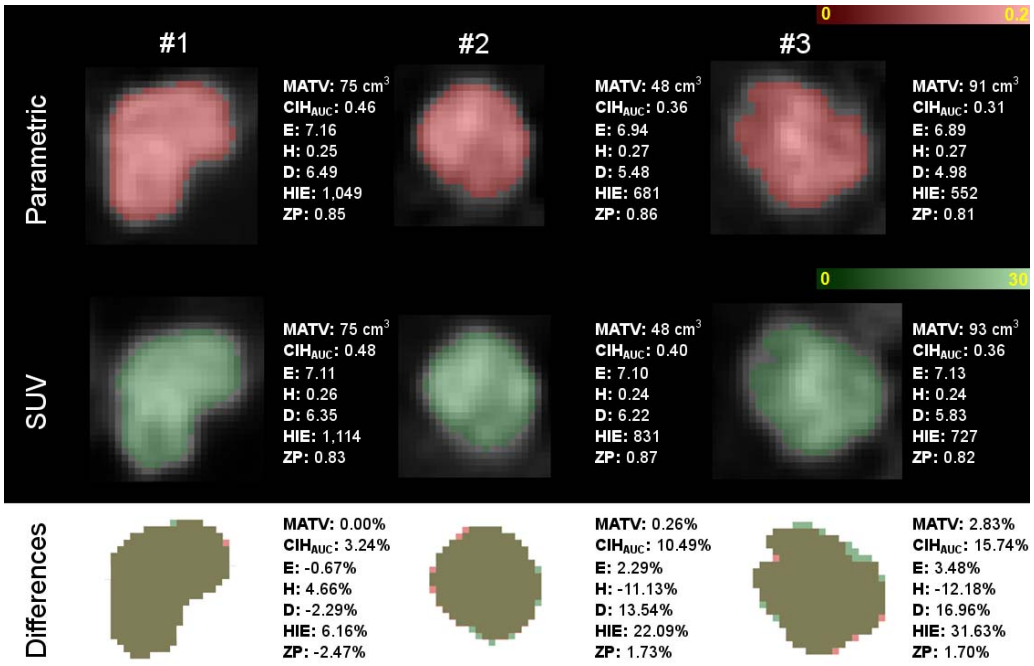

Figure 1: *Three different tumor examples with parametric Ki and SUV images in the upper and middle row respectively and differences between the two images in the bottom row. Examples 1, 2 and 3 correspond to cases with small, medium and large differences between parametric Ki and static SUV images respectively.*

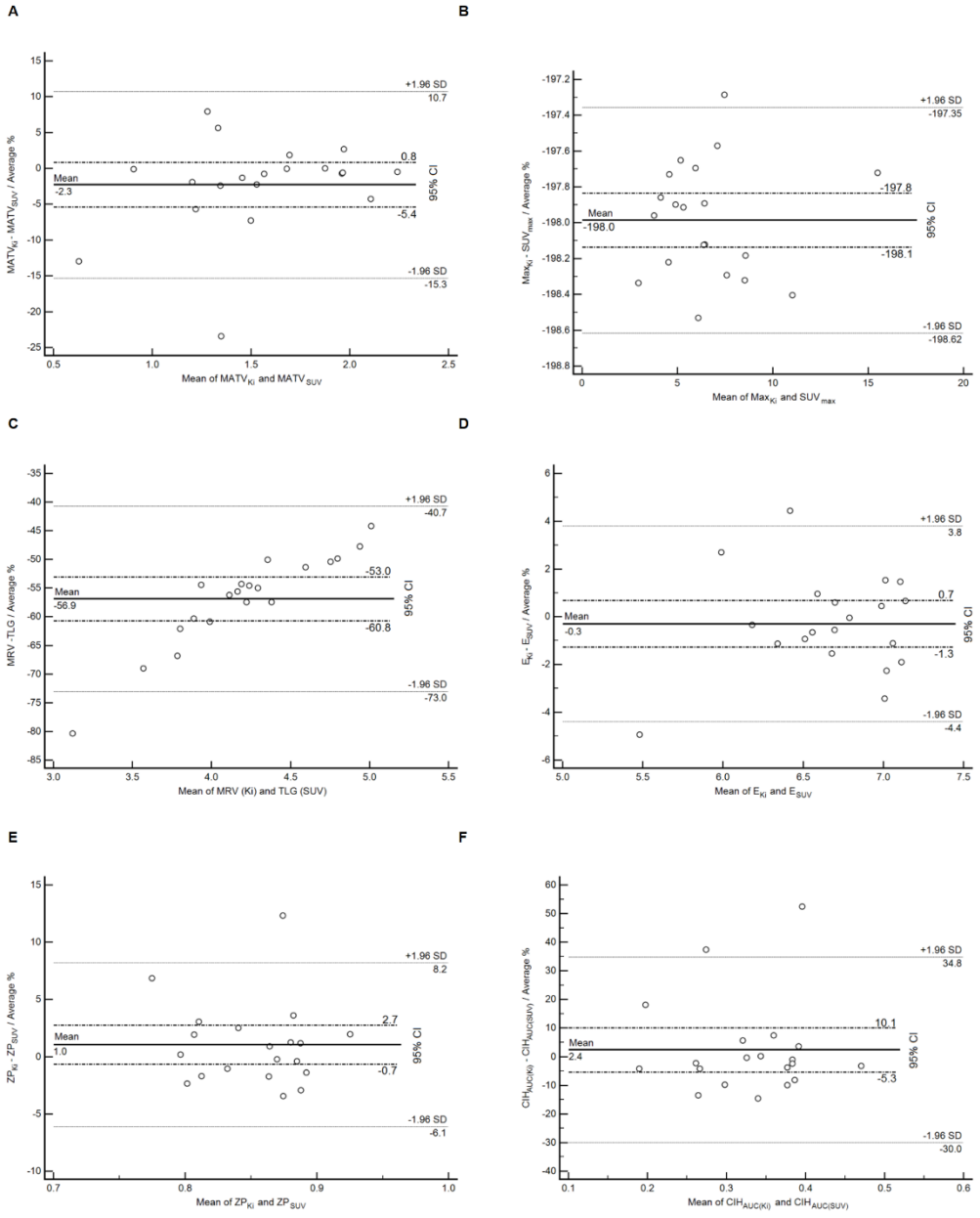

Figure 2: *Bland-Altman plot of MATV (logarithmic transformation) (A), CIH_{AUC} (B), SUV_{max}/maximum K_i (C), TLG/MRV (logarithmic transformation) (D), Entropy (E), ZP (F)*. For each graph mean value, +/- 1.96 standard deviation (SD) and 95% confidence interval for the mean of differences is reported.

Tables

Parameter:	**Value:**
Male [%]:	70
Mean age {range} [year]:	63.4 {44.3-77.8}
Mean body mass {stdev} [kg]:	78.2 {15.1}
Mean BMI {stdev} [kg/m^2]:	26.0 {5.3}
Mean mass activity {stdev} [MBq/kg]:	3.32 {0.42}*
Median serum glucose level {range} [mmol/L]:	5.3 {4.5-7.7}
Location [%]:	
- *Right upper lobe*	50
- *Right middle lobe*	5
- *Right lower lobe*	0
- *Left upper lobe*	35
- *Left lower lobe*	10
Treatment [%]:	
- *Lobectomy R0*	85
- *Pneumonectomy R0*	15
Histology (NSCLC) [%]:	
- *Squamous Cell carcinoma*	60
- *Adenocarcinoma*	30
- No mucinous differentiation	20
- Partially mucinous	5
- Mucinous differentiation	5
- *Sarcomatoid pleiomorph carcinoma*	5
- *Neuro-endocrine carcinoma*	5
Differentiation [%]:	
- *Poor*	55
- *Moderate*	30
- *Unknown*	15
Mean Histological tumor diameter {range} [mm]	52.3 {15.0-85.0}**
TNM-classification [%] :	
- *T2N0M0 (stage IB)*	30
- *T3N0M0 (stage IIB)*	30
- *T2N1M0 (stage IIB)*	40

*Table 1 : Patient characteristics (n=20). BMI : body mass index ; R0 : resection margins free of tumor ; stdev: standard-deviation; *p=0.193 for a 2-tailed one-sample t-test compared with reference mass activity of 3.45MBq/kg; **one lesion was smaller than 30mm at final histology, it was larger than 30mm at CT due to surrounding organizing pneumoni*

	Parametric				Static			
	25%	median	75%	normality	25%	median	75%	normality
MATV (cm^3)	18.43	49.51	82.47	0,01	18.83	35.39	81.29	0.006
CIH_{AUC}	0.27	0.30	0.35	>0.10	0.28	0.33	0.38	>0.10
Entropy (E)	4.52	4.69	5.18	>0.10	6.46	6.72	7.08	>0.10
Homogeneity (H)	0.51	0.55	0.56	0,0083	0.22	0.25	0.28	>0.10
Dissimilarity (D)	2.03	2.22	2.48	>0.10	4.86	6.07	7.26	>0.10
High intensity emphasis (HIE)	854	1108	1229	>0.10	514	661	800	>0.10
Zone percentage (ZP)	0.41	0.47	0.51	>0.10	0.82	0.86	0.88	>0.10
SUV_{max}/Ki_{max}	0.05	0.06	0.07	0.06	9.41	12.41	14.96	>0.10
TLG/MRIV	161	448	1074	0,0002	1,13E+05	2,29E+05	5,14E+05	0.0001

Table 2: Statistics and normality (Kolmogorov-Smirnov test) for features derived from static and parametric ^{18}F-FDG PET images

	Bland-Altman analysis							Spearman rank correlation		
	% difference		P-value							
	Mean	SD	(H0: Mean=0)	LL	95% CI for LL	UL	95% CI for UL	rs	p-value	95% CI
MATV (cm^3)*	-2.31	6.64	0.14	-15.32	-20.72 to -9.91	10.71	5.30 to 16.11	0.96	<0.0001	0.90 to 0.99
CIH_{AUC}	2.39	16.52	0.53	-29.99	-43.43 to -16.55	34.77	21.33 to 48.21	0.75	0.0002	0.45 to 0.89
Entropy (E)	-0.30	2.09	0.53	-4.39	-6.09 to -2.69	3.80	2.10 to 5.49	0.91	<0.0001	0.78 to 0.96
Homogeneity (H)	0.64	11.91	0.81	-22.71	-32.40 to -13.02	23.99	14.30 to 33.68	0.70	0.0006	0.38 to 0.87
Dissimilarity (D)	-1.13	16.30	0.76	-33.08	-46.34 to -19.82	30.82	17.55 to 44.08	0.78	<0.0001	0.52 to 0.91
High intensity emphasis (HIE)	0.32	20.89	0.95	-40.63	-57.63 to -23.63	41.27	24.27 to 58.26	0.77	0.0001	0.51 to 0.91
Zone percentage (ZP)	1.04	3.65	0.22	-6.11	-9.07 to -3.14	8.18	5.22 to 11.15	0.74	0.0002	0.44 to 0.89
SUV_{max}/Ki_{max}	-	-	-	-	-	-	-	0.90	<0.0001	0.76 to 0.96
TLG/MRV*	-	-	-	-	-	-	-	0.98	<0.0001	0.94 to 0.99

*Table 3: Results from the Bland-Altman analysis (*TLG/MRV and MATV were log transformed) and the Spearman rank correlation, between features from static and parametric ^{18}F-FDG PET images*